# $p27^{Kip1}$ Repression of ErbB2-Induced Mammary Tumor Growth in Transgenic Mice Involves Skp2 and Wnt/β-Catenin Signaling

James Hulit,[1] Richard J. Lee,[1] Zhiping Li,[2] Chenguang Wang,[2] Sanjay Katiyar,[2] Jianguo Yang,[2] Andrew A. Quong,[2] Kongming Wu,[2] Chris Albanese,[3] Robert Russell,[3] Dolores Di Vizio,[1] Andrew Koff,[3] Saiinder Thummala,[1] Hui Zhang,[4,6] Jennifer Harrell,[6] Hong Sun,[6] William J. Muller,[7] Giorgio Inghirami,[5] Michael P. Lisanti,[2] and Richard G. Pestell[2]

[1]Department of Developmental and Molecular Biology, Department of Medicine, Albert Einstein College of Medicine, Bronx, New York; [2]Kimmel Cancer Center, Departments of Cancer Biology and Medical Oncology, Thomas Jefferson University, Philadelphia, Pennsylvania; [3]Department of Oncology, Lombardi Comprehensive Cancer Center, Georgetown University, Washington, District of Columbia; [4]Molecular Biology Program, Memorial Sloan-Kettering Cancer Center, Sloan-Kettering Institute; [5]Department of Pathology and Kaplan Comprehensive Cancer Center, New York University School of Medicine, New York, New York; [6]Department of Genetics, Yale University School of Medicine, New Haven, Connecticut; and [7]Molecular Oncology Labs, Royal Victoria Hospital, McGill University, Montreal, Quebec, Canada

## Abstract

**Expression of the cyclin-dependent kinase (Cdk) inhibitor ($p27^{Kip1}$) is frequently reduced in human tumors, often correlating with poor prognosis. $p27^{Kip1}$ functions as a haploinsufficient tumor suppressor; however, the mechanism by which one allele of $p27^{Kip1}$ regulates oncogenic signaling *in vivo* is not well understood. We therefore investigated the mechanisms by which $p27^{Kip1}$ inhibits mammary tumor onset. Using the common background strain of FVB, $p27^{Kip1}$ heterozygosity ($p27^{+/-}$) accelerated ErbB2-induced mammary tumorigenesis. We conducted microarray analyses of mammary tumors developing in mice with genetic haploinsufficiency for $p27^{Kip1}$ expressing a mammary-targeted ErbB2 oncogene. Global gene expression profiling and Western blot analysis of ErbB2/$p27^{+/-}$ tumors showed that the loss of $p27^{Kip1}$ induced genes promoting lymphangiogenesis, cellular proliferation, and collaborative oncogenic signaling (*Wnt/β-catenin/Tcf, Cdc25a, Smad7*, and *Skp2*). Skp2 expression was induced by ErbB2 and repressed by $p27^{Kip1}$. Degradation of $p27^{Kip1}$ involves an SCF-type E3 ubiquitin ligase, including Skp2. The Skp2 component of the $SCF^{SKP2}$ complex that degrades $p27^{Kip1}$ was increased in ErbB2 tumors correlating with earlier tumor onset. In both murine and human ErbB2-overexpressing breast cancers, $p27^{Kip1}$ levels correlated inversely with Skp2. $p27^{Kip1}$ haploinsufficiency activated Wnt/β-catenin/hedgehog signaling. Reintroduction of $p27^{Kip1}$ inhibited β-catenin induction of Tcf-responsive genes (*Siamosis, c-Myc*, and *Smad7*). $p27^{Kip1}$ is haploinsufficient for ErbB2 mammary tumor suppression *in vivo* and functions to repress collaborative oncogenic signals including Skp2 and Wnt/β-catenin signaling.** (Cancer Res 2006; 66(17): 8529-41)

## Introduction

Cellular proliferation is positively regulated by cyclin/cyclin-dependent kinase (Cdk) complexes, which are opposed by the Cdk inhibitors. The Cdk inhibitors are classified into two families: p21 ($p21^{Cip1}$, $p27^{Kip1}$, and $p57^{Kip2}$) and $p16^{INK4a}$ (*p15, p16, p18*, and *p19*). $p27^{Kip1}$ inhibits most cyclin/Cdk complexes, in particular cyclin E/Cdk2. Expression of $p27^{Kip1}$ in cell lines causes cell cycle arrest. Mitogen withdrawal and cadherin-mediated cell contact inhibition induce $p27^{Kip1}$ binding to cyclin E/Cdk2 and cyclin A/Cdk2, correlating with the inhibition of cell cycle progression and DNA synthesis. $p27^{Kip1}$ regulates cellular polarity and inhibits cell migration induced by cell-extracellular matrix contact. $p27^{Kip1}$ abundance is regulated at the level of translation and protein turnover. Phosphorylation of $p27^{Kip1}$ by Cdk2 creates a binding site for a specific SCF-type E3 ubiquitin-protein ligase, which promotes proteosome-mediated degradation of $p27^{Kip1}$ (1–3). The F-box protein Skp2 is the substrate recognition factor of the SCF complex, which recognizes and binds to phosphorylated $p27^{Kip1}$. Skp2 is required for $G_1$-S phase transition in transformed cells and diploid fibroblasts (4) and Skp2-deficient cells exhibit increased $p27^{Kip1}$ levels and polyploidy (5).

The mechanisms by which $p27^{Kip1}$ regulates tumorigenesis are less well understood. In the majority of studies, reduced $p27^{Kip1}$ levels in tumors, including colon and breast cancers, correlates with poor prognosis, although elevated levels are reported in a subset of tumors (6–9). Reduction in $p27^{Kip1}$ expression in tumors correlates with tumor agressivenesss and dedifferentiation. Point mutations in the coding region of the $p27^{Kip1}$ gene are rare in human tumors, although loss of heterozygosity has been observed (10–14). Despite the widespread implication that $p27^{Kip1}$ may serve as a tumor suppressor in different human cancers (15, 16), inactivation of *Cdkn1b* (encoding $p27^{Kip1}$) in mice does not result in enhanced spontaneous tumor onset, with the exception of pituitary adenomas (17–19). $p27^{Kip1}$ deficiency accelerated gastrointestinal neoplasia induced by 1,2-dimethylhydrazine or by mutation of the *Apc* gene in the *Min* mice (20). Reduced $p27^{Kip1}$ may be anticipated to cooperate as a component of multistep tumorigenesis with loss of other tumor suppressors or activating oncogenes. The inactivation of $p27^{Kip1}$, for example, may be epistatic to the inactivation of *pten*, as the inactivation of one *pten* allele, together with the inactivation of one *Cdkn1b* allele, enhances the rate of prostate tumor onset (21).

The *neu* (c-*ErbB2, HER-2*) proto-oncogene encodes a receptor tyrosine kinase that is a member of a growth factor receptor family, which is overexpressed in 20% to 30% of human breast tumors (22). When under the control of the murine mammary tumor virus (MMTV) long terminal repeat, overexpression of either wild-type or

**Note:** Supplementary data for this article are available at Cancer Research Online (http://cancerres.aacrjournals.org/).

J. Hulit and R.J. Lee contributed equally to the manuscript.

**Requests for reprints:** Richard G. Pestell, Departments of Cancer Biology and Medical Oncology, Thomas Jefferson University, 233 South 10th Street, Philadelphia, PA 19107. Phone: 215-503-5649; Fax: 215-923-9334; E-mail: Richard.Pestell@jefferson.edu or D_Scardino@mail.jci.tju.edu.



doi:10.1158/0008-5472.CAN-06-0149

activated ErbB2 induces mammary adenocarcinomas in transgenic mice with high frequency (23, 24). Several cell cycle components regulated by ErbB2 have been implicated in mammary tumorigenesis. Cyclin D1 is overexpressed in MMTV-ErbB2 mammary tumors (25). In contrast to cyclin E or cyclin A, cyclin D1 is selectively transcriptionally induced by ErbB2 (25) and cyclin D1 antisense is sufficient to abrogate MMTV-ErbB2 induced cellular growth in nude mice (25). Furthermore, *cyclin D1*$^{-/-}$ mice are resistant to tumor induction by ErbB2 (26). In cultured cells, heregulin engagement and activation of ErbB2 correlate with a reduction in p27$^{Kip1}$ protein abundance (27). Conversely, ErbB2 inhibitor antibodies increase p27$^{Kip1}$ abundance, thus implicating p27$^{Kip1}$ in ErbB2 mammary epithelial cell proliferation.

In these studies, we have examined the *in vivo* functions of p27$^{Kip1}$ in mammary gland tumorigenesis by mating mice homozygously deleted of *Cdkn1b* (*p27$^{Kip1}$*) with transgenic mice expressing mammary-targeted oncogenic ErbB2. We show that *p27$^{Kip1}$* is haploinsufficient for ErbB2 mammary tumor suppression *in vivo*. The loss of a single *p27$^{Kip1}$* allele resulted in a disproportionate decrease (~80%) in p27$^{Kip1}$ abundance and increased Skp2. Global gene expression profiling and Western blot analysis of ErbB2/p27$^{+/-}$ tumors showed that the loss of p27$^{Kip1}$ induced genes promoting Wnt/β-catenin/hedgehog signaling (*Dhh, Wnt3*, and *Lef1*), lymphangiogenesis (*Flt3l* and *EphA2*), cellular proliferation, and collaborative oncogenic signaling (*Cdc25A, Smad7*, and *Skp2*). Reintroduction of p27$^{Kip1}$ into p27$^{Kip1}$-deficient cells inhibited expression of Skp2, Smad7, and Wnt/β-catenin responsive genes. Thus, p27$^{Kip1}$ inhibits Skp2, Smad7, and Wnt/β-catenin responsive genes through a mechanism that involves repression of target gene promoter activity.

## Materials and Methods

### Animals

MMTV-*neu* mice (24) and mice homozygously deleted of the gene encoding p27$^{Kip1}$ were previously described (17). The MMTV-*neu* mice were in the FVB strain and the *p27$^{Kip1-/-}$* mice on the C57BL/6 background were backcrossed for three generations into FVB and then backcrossed into the MMTV-*neu* mice of FVB strain. Animal care was conducted in accordance with the standards set forth by the Institute for Animal Studies of the Albert Einstein College of Medicine. For genomic analyses of the transgenic mice, weaned animals were identified through a system of toe tagging. One centimeter of tail section was removed to make genomic DNA. Tail sections were incubated overnight at 50°C to 55°C in 700 μL of a proteolytic solution [50 mmol/L Tris (pH 8.0), 100 mmol/L EDTA, and 0.5% SDS] plus 20 μL of 20 mg/mL proteinase K solution. DNA was purified by phenol/chloroform extraction and ethanol precipitation, followed by resuspension in 250 μL of 0.1× TE (10 mmol/L Tris, 1 mmol/L EDTA). Virgin female *neu-p27$^{Kip1}$* mice were finger palpated over the length of their ventral side biweekly. On detection of a mass, individual mice of each specific *p27$^{Kip1}$* genotype were scored against the entire population of that genotype which remained at that time point and charted.

### PCR

PCR primers for p27$^{Kip1}$ from the *p27$^{Kip1}$*-null mice were SW39, 5′-ATATTGCTGAAGAGCTTGGCGG; SW40, 5′-TCAAACGTGAGAGTGTC-TAACGG; and SW41, 5′-AGGGGCTTATGATTCTGAAAGTCG. For detection of the wild-type and heterozygote *p27$^{Kip1}$* alleles, the primers SW39 (a forward primer that binds nucleotides 1,420-1,441 of PMC1POLA), SW40 (a forward primer binding nucleotides 4-26 of pλ-$^{KIP1}$-34-1), and SW41 (a reverse primer binding nucleotides 209-186 of pλ-$^{KIP1}$-34-1) were used. When used in conjunction, SW40 and SW41 amplify a region of 206 bp from the wild-type locus, whereas SW40 and SW39 produce a 298-bp product from the mutant locus. The reaction for each genomic DNA sample included 1 μg of genomic DNA, 100 pmol SW40, 50 pmol SW39, 50 pmol SW41, 1.5 units of Taq polymerase (Fisher Scientific, Pittsburgh, PA), 200 μmol/L of each deoxynucleotide triphosphate (dNTP), and PCR buffer [40 mmol/L NaCl, 10 mmol/L Tris (pH 8.9), 1.5 mmol/L $MgCl_2$, and 0.01% gelatin]. Genomic DNA (denatured at 99°C, 4 minutes; 4°C, 1 minute) was subjected to PCR (35 cycles at 94°C, 60°C, and 72°C, 1 minute each).

PCR primer sequences used for *neu* from the MMTV-*neu* mice were 5′-CGGAACCCACATCAGGCC and 5′-TTTCCTGCAGCCTACGC. For detection of the *neu* transgene, the same buffer conditions were used as above, with the forward and reverse primers specific for *neu*. The PCR program was 30 cycles of 94°C, 1 minute; 92°C, 30 seconds; 58°C, 30 seconds; and 72°C, 1 minute.

### Southern Blots

For detection of the *neu* transgene, 10 μg of genomic DNA were digested with *Bam*H1 overnight at 37°C in 200 μL of total volume until complete digestion was confirmed with 5% of the reaction mixture. DNA was ethanol precipitated, resuspended in 15 to 20 μL of volume, and electrophoresed in a 1% agarose gel using proper controls and markers. After image verification, the gel was denatured for at least 45 minutes in 1.5 mol/L NaCl and 0.4 N NaOH, rinsed with water, and neutralized for at least 45 minutes in 1.5 mol/L NaCl and 0.5 mol/L Tris (pH 7.6). DNA was transferred overnight onto Hybond-N (charged nylon) membrane [equilibrated in 20× SSC (175.3 g of NaCl and 88.2 g of sodium citrate in 1 liter of water)]. DNA was then UV cross-linked to the nylon membrane. The *neu*-specific probe was prepared by gel purification of an 800-bp fragment from a *Bam*H1-digested pJ4ΩNeuN plasmid. Twenty-five nanograms of probe were labeled with [α-$^{32}$P]dCTP using the Amersham Redi-Prime kit protocol and the probe solution was prepared with RapidHyb solution according to the protocol of the manufacturer (Amersham Pharmacia Biotech, Piscataway, NJ). The membrane was hybridized with probe at 65°C for 3 hours with shaking, washed twice for 5 minutes each using 2× SSC and 0.1% SDS at room temperature, twice for 5 minutes with 0.2× SSC and 0.1% SDS at room temperature, and twice for 5 minutes with 0.2× SSC and 0.1% SDS at 65°C. Blots were then exposed to film or phosphorimaging screen (Molecular Dynamics, Sunnyvale, CA).

### Whole-Mount Mammary Gland Preparation

Fourth (abdominal) mammary glands were surgically removed, stretched, and mounted onto glass slides, followed by fixation in 75% ethanol/25% acetic acid overnight. Tissues were then washed in 70% ethanol, followed by 5 minutes in distilled water, and stained overnight in an aluminum-carmine dye solution (1 g carmine dye, 2.5 g potassium alum; Sigma Chemical, St. Louis, MO) diluted in 500 mL of water. The solution was brought to a boil, followed by addition of a few thymol crystals (Sigma) while stirring. The solution was filtered and stored at 4°C. Following staining, mammary glands were dehydrated through a graded series of ethanol solutions (15 minutes each at 70%, 90%, and 100%), defatted in xylenes (Electron Microscopy Sciences, Fort Washington, PA), and stored in methyl salicylate (Sigma). Ductal branch points in the mammary gland whole-mount preparations were measured from the nipple area to the tip of the three longest ducts passing through the lymph node. The numbers of branches represent the mean branching number along the three longest ducts. Epithelial cell area was determined from the cross-sectional area of ductal end points. Area measurements were assessed in 10 separate animals (age, 165 days) using 181 fields and analyzed with NIH image software, with the data being expressed as total pixel units. Statistical evaluations were done with either two-tailed Student's *t* test or Mann-Whitney *U* test in cases where the data could not be assumed to be Gaussian.

### Nucleus Size Analysis

H&E-stained mammary tumor sections were analyzed by microscopy using Nikon model Diaphop 300 system (Nikon Instruments, Inc., Melville, NY) at 40× objective. Images were captured with the SPOT charge-coupled device digital camera (model 1.5.0, Diagnostic Instruments, Inc., Sterling Heights, MI) fitted with a Nikon 0.45× HRD045-NIK lens. Digital imaging, capture, and editing were done with Adobe Photoshop (Adobe Systems, Inc., San Jose CA). Nucleus counting and measuring were done with Image-Pro

Plus version 3.0 (Media Cybernetics, Silver Spring, MD). Nucleus number and area data were graphically analyzed and displayed using Microsoft Excel (Microsoft Corporation, Redmond, WA). Briefly, three fields were selected from each section; the images were captured and saved as gray scale TIFF files. Images were then transformed into a two-color display (black nuclei and white background). Files were then imported into the Image-Pro software program. Nuclei were then analyzed for both number and area (area displayed as total number of pixels).

### Western Blots

The abundance of mitogen-activated protein kinase and cell cycle–, survival-, and apoptosis-related proteins was determined by Western blot analysis as previously described (25). Antibodies included anti-cyclin D1 (Ab3; NeoMarkers, Fremont, CA), anti-$p27^{Kip1}$ (F-8; Santa Cruz Biotechnology, Santa Cruz, CA), anti-$p21^{Cip1}$ (187; Santa Cruz Biotechnology), anti-cyclin E (HE111; Santa Cruz Biotechnology), anti-Cul-1 (C20; Santa Cruz Biotechnology), anti-Akt and anti-phospho-Akt (9272 and serine 473; Cell Signaling Technology, Danvers, MA), and a guanine nucleotide dissociation inhibitor antibody (a generous gift from Perry Bickel, Washington University, St. Louis, MO).

### Immunohistochemistry

For analysis of murine mammary tumors, paraffin-embedded sections were stained and visualized with a 3,3′-diaminobenzidine (DAB) method (Dako Kit LSAB+, peroxidase) as detailed in a protocol provided by the manufacturer (Dako Corporation, Carpinteria, CA). Antibodies used were directed to cyclin D1 (25) or $p27^{Kip1}$ (1:500 dilution; Transduction Laboratories, Inc., BD Biosciences, Franklin Lakes, NJ). Briefly, after deparaffination, antigens were retrieved by microwave irradiation in 0.01 mol/L trisodium citrate buffer (pH 6.0). Slides were washed and incubated with primary antibodies for 1 hour at room temperature, followed by incubation with secondary antibodies. Positive signals were revealed by DAB chromogen according to the conditions of the supplier. Slides were then counterstained with Harris hematoxylin (Fisher Scientific). For analysis of human breast cancer tumors, immunohistochemical staining for Skp2 was done with a mix of four different affinity-purified monoclonal antibodies (mAb) as previously described (28). At least 20 high-power fields were chosen at random and 2,000 cells were counted. Immunostaining was done on formalin-fixed, paraffin-embedded tissues with the avidin-biotin-peroxidase complex method and a semiautomated immunostainer (DAKO or Ventana System) as described (29). Antigen retrieval was done by microwaving the slides for 20 minutes in 10 mmol/L citrate buffer (pH 8.0 for Skp2; Zymed, South San Francisco, CA) or for 16 minutes in Trilogy buffer (Cell Marque, Los Angeles, CA; cb11, Novacastra, New Castle, United Kingdom). Immunostaining was evaluated by a pathologist blinded to the conditions. At least 10 high-power fields were chosen randomly and >100 cells per field were counted. The tumors were scored as percentage of positive cells for each antigen. The determination of HER-2 protein overexpression was based on the membrane staining only. Cytoplasmic staining was considered nonspecific. Immunohistochemical values for HER-2 overexpression were expressed as negative (0 and +), weakly positive (++), and strongly positive (+++).

**Plasmids and reporter constructs.** Luciferase reporter genes c-Myc-LUC, c-Myc ΔTcf-LUC (30), Siamosis-LUC, Siamosis ΔTcf-LUC (31), Engr-LUC, Engr-ΔTcf (30), Smad7 (−4,600 to +672), Smad7Δ (−303 to +672; ref. 32), pCGT-Skp2 construct expression vector (33), CMV-Skp2 (34), β-catenin S33 (35), and PSV2 Neu NT (25). A 1.87-kb Skp2 promoter fragment was cloned into pGL3-LUC to form −1870 Skp2-LUC.

**Cell culture and reporter assays.** The $p27^{Kip1-/-}$ 3T3 and $p27^{Kip+/+}$ 3T3 were maintained in DMEM with 10% FCS and 1% penicillin/streptomycin at 37°C under 10% $CO_2$. Luciferase assay procedures were done as previously described (36). Cells were plated in 12-well dishes (Falcon) and seeded at 50% to 70% confluency the night before. Transfections were carried out with Polyfect Transfection reagent (Qiagen, Valencia, CA). Transfection protocol was based on the instructions of the manufacturer. Vectors were individually aliquoted into 1.5-mL tubes (Eppendorf) and diluted to 150 μL with serum- and antibiotic-free DMEM. To the DNA/DMEM mixture was added 10 μL of Polyfect reagent per reaction tube. After 10 minutes of incubation, 1.0 mL of full mediun (serum plus antibiotics) was added to the DNA/Polyfect mixture and immediately transferred onto cells that had been washed with PBS. Luciferase activity was determined 24 to 36 hours posttransfection. Renilla luciferase (TK-LUC) was cotransfected (in a 1:10 ratio with reporter vector) as an internal control for transfection efficiency. Luciferase assays were done at room temperature with Autolumat LB 953 (EG&G Berthold, Berthold Technologies, Oak Ridge, TN). Measurements were made over 10 seconds to assess luciferase content. Data values were expressed in arbitrary light units. Background activity from cell extracts was typically <100 arbitrary light units/10 s. Statistical analyses were done with the Mann-Whitney $U$ test and significant differences were established as $P < 0.05$. Luciferase buffers and reagents were purchased from Promega (Madison, WI).

### cDNA and Oligonucleotide Microarray Analyses

RNA was isolated from freshly dissected mammary tumors from MMTV-ErbB2 transgenic mice of either $p27^{+/-}$ or $p27^{+/+}$ allele type. The mRNA was examined with the cDNA microarray glass slides or Affymetrix oligonucleotide arrays to expand the number of genes examined. Affymetrix Mu11K A/B GeneChips were used for all oligonucleotide microarray experiments. The targets for Affymetrix DNA microarray analysis were prepared as described by the manufacturer. Briefly, double-stranded cDNA was synthesized from total RNA (10 μg starting material) isolated from tissue culture harvests. Biotin-labeled cRNA was generated by *in vitro* transcription from the DNA. The cRNA was fragmented before hybridization. A hybridization cocktail was prepared that included the fragmented cRNA, probe array controls, bovine serum albumin, and herring sperm DNA. The cRNA was hybridized to the array oligonucleotide probes for a 16-hour incubation at 45°C. Immediately after the hybridization, the hybridized probe array underwent automated washing and staining on Affymetrix Fluidics Station. The DNA chips were scanned with the Affymetrix GeneChip scanner and the signals processed with the GeneChip expression analysis algorithm v.2 (Affymetrix, Santa Clara, CA). Metagene regression analysis of expression data was conducted as previously described (25, 37). Affymetrix U74 Av2 data sets were processed with Affymetrix MAS5.0 to compute signal values for each probe set and resulting data sets for each specimen. Details on the methods of normalization, calculation of geometric fold changes, $t$ test analyses, and hierarchical clustering were previously described (38).

Unique human expressed sequence tags (16,580) from Research Genetics (Huntsville, AL) were used as cDNA probes, which were spotted on two separate glass slides: 5H arrays contained 7,873 non-sequence-verified probes and H1 arrays contained 8,707 sequence-verified probed.[8] For each hybridization, cDNA targets were prepared from the RNA sample (Cy3 labeled) obtained from ErbB2/$p27^{+/-}$ cells and the reference RNA sample (Cy3-labeled ErbB2 $p27^{+/+}$). RNA was subjected to *in vitro* transcription in the presence of biotinylated Cy3-UTP or Cy5-UTP (Amersham Pharmacia Biotech). The target was hybridized for 12 hours at 50°C to the arrays. Independent images were obtained from Cy3 and Cy5 fluorescence emitted from hybridized microarrays using a custom-built dual channel laser scanning microscope.[9] ScanAlyze version 2.44 software (M. Eisen, Stanford University, Palo Alto, CA)[10] was used as described in the ScanAlyze manual to generate raw data files containing measurements of signal and background fluorescence emissions of Cy3 and Cy5, respectively, for each element. Genes were identified after eliminating genes that failed to vary in expression level within an experiment by a factor of 2 and an absolute value of 100 and normalizing within experiments to a mean of 0 and an SD of 1.

Genes were selected based on the criteria that $P < 0.05$ from a two-tailed $t$ test and the fold change was >1.8 over the three replicates. This set of genes is listed in Fig. 5 as a heat map, where data from each probe are

[8] Detailed descriptions of microarray hardware and procedures are available from http://www.aecom.yu.edu/home/molgen/facilities.html.
[9] See http://www.aecom.yu.edu/home/molgen/facilities.html for specifications.
[10] http://www.microarrays.org/software.html.

**Table 1.** Differentially expressed genes

| Symbol | Fold change | Gene assignment | Function/activity/tissue | Cluster category | GenBank accession no. |
|---|---|---|---|---|---|
| Genes up-regulated | | | | | |
| *Shmt1* | 1.87 | serine hydroxymethyl transferase 1 (soluble) | hydroxymethyltransferase | amino acid metabolism | X94478 |
| *Pald* | 2.78 | paladin | protein Tyr/Ser/Thr phosphatase | amino acid metabolism | AV266918 |
| *Tyrp1* | 4.89 | tyrosinase-related protein 1 | monooxygenase, melanin biosynthesis | amino acid metabolism | AV237026 |
| *Agtrap* | 1.82 | angiotensin II, type I receptor-associated protein | receptor | cardiovascular regulation | AA407794 |
| *Pcdha11* | 1.85 | protocadherin α11 | calcium binding | cell adhesion | AB008182 |
| *SMAF1* | 2.28 | SMAF1 | transactivation | cell determination | AI118905 |
| *Gap43* | 2.07 | growth associated protein 43/neuromodulin | nerve growth factor pathway/ neuron outgrowth | cell growth | AI841303 |
| *Nfatc2* | 2.22 | nuclear factor of activated T-cells, cytoplasmic 2 | transcription factor-muscle | cell growth | U36576 |
| *Tmeff2* | 4.6 | transmembrane protein with epidermal growth factor–like and two follistatin-like domains 2 | serine protease inhibitor | cell growth | AB017270 |
| *Cdc25a* | 6.15 | cell division cycle 25 homologue A (*S. cerevisiae*) | protein tyrosine phosphatase | cell growth | AV315419 |
| *Dusp9* | 2.36 | dual specificity phosphatase 9 | protein phosphatase | cell growth regulation | AV225351 |
| *Wnt3* | 1.78 | wingless-related MMTV integration site 3 | receptor ligand | cell growth / maintenance | M32502 |
| *Igf2bp1* | 1.79 | insulin-like growth factor 2, binding protein 1 | signal transduction pathway | cell growth/ maintenance | AF061569 |
| *Flt3l* | 3.9 | FMS-like tyrosine kinase 3 ligand | cytokine | cell growth/ maintenance | L23636 |
| *Epha2* | 2.12 | Eph receptor A2 | receptor tyrosine-kinase | cell growth/ positioning | U07634 |
| *Ptk2* | 2.28 | protein tyrosine kinase 2 | protein tyrosine kinase-focal contacts | cell motility | AV233274 |
| *Mcl1* | 2.5 | myeloid cell leukemia sequence 1 | antiapoptotic factor-myeloid | cell survival | AV257057 |
| *Dhh* | 1.84 | desert hedgehog | peptidase | cell-cell signaling | AV321877 |
| *Tekt1* | 3.45 | tektin 1 | filament forming protein-spermatocytes | cytoskeleton dynamics | AF081947 |
| *Lhx1* | 1.81 | LIM homeobox protein 1 | transcription factor | development | Z27410 |
| *Six3* | 3.55 | sine oculis-related homeobox 3 homologue (*Drosophila*) | transactivation, inhibitory toward Wnt1 expression | development | X90871 |
| *Tk1* | 2.66 | thymidine kinase 1 | thymidine kinase | DNA biosynthesis | AV227393 |
| *4733401H14Rik* | 2.23 | RIKEN cDNA 4733401H14 gene | DNase | DNA metabolism | AA607761 |
| *Ddx25* | 2.6 | DEAD/H (Asp-Glu-Ala-Asp/His) box polypeptide 25 | helicase | DNA replication | AA982686 |
| *Odz4/Doc4* | 1.79 | odd Oz/ten-m homologue 4 (*Drosophila*) | pair-rule gene homologue | ER stress response | AB025413 |
| *Elovl3* | 2.51 | elongation of very long chain fatty acids-like 3 | integral ER protein | fatty acid metabolism | U97107 |
| *C9* | 2.11 | complement component 9 | part of complement membrane attack complex | immune response | X05475 |
| | 2.51 | MCT8_MOUSE Mast cell protease 8 precursor (MMCP-8) | protease | immune response | AV373223 |
| *S100a9* | 3.23 | S100 calcium binding protein A9 (calgranulin B) | macrophage expressed during inflammation | immune response | M83219 |
| *Cd97* | 4.06 | CD97 antigen | G-protein coupled receptor | immune response | Y18365 |
| *Il4* | 6.61 | interleukin 4 | cytokine/B cell activation | immune response | X03532 |
| *Slc9a1* | 1.94 | solute carrier family 9 (sodium/hydrogen exchanger), member 1 | ion channel | membrane transport | U51112 |
| *Viaat* | 1.97 | vesicular inhibitory amino acid transporter | γ-aminobutyric acid (γ-GABA) and glycine transporter-neural tissue | membrane transport | AJ001598 |

(*Continued on the following page*)

**Table 1.** Differentially expressed genes (Cont'd)

| Symbol | Fold change | Gene assignment | Function/activity/tissue | Cluster category | GenBank accession no. |
|---|---|---|---|---|---|
| *Gria4* | 2.15 | glutamate receptor, ionotropic, AMPA4 (α4) | ion channel | membrane transport | AB022913 |
| *Ryr2* | 3.07 | ryanodine receptor 2, cardiac | ion channel-cardiac | membrane transport | X78667 |
| *Nudel-pending* | 3.3 | nuclear distribution gene E-like | retrograde axon cargo transport | microtubule transport | AW047320 |
| *Skd3* | 1.9 | suppressor of $K^+$ transport defect 3 | transcription factor | mitochondrial biogenesis | AV332176 |
| *Mrg1* | 2.04 | myeloid ecotropic viral integration site-related gene 1 | transcription factor | morphogenesis | U68383 |
| *Pcsk4* | 2.34 | proprotein convertase subtilisin/ kexin type 4 | convertase | protein degradation | D01093 |
| *Mmp16* | 1.88 | matrix metalloproteinase 16 | metallopeptidase | protein processing | AB021228 |
| *Cct6a* | 1.99 | chaperonin subunit 6a (ζ) | protein folding | protein processing | Z31557 |
| *Rab3a* | 4.18 | RAB3A, member RAS oncogene family | small monomeric GTPase | protein trafficking | AV347669 |
| Genes down-regulated | | | | | |
| *Prkcm* | −2.34 | protein kinase C, μ | tyrosine kinase | cell growth/maintenance | Z34524 |
| *Mras* | −2.7 | muscle and microspikes RAS | small GTPase | cell growth/maintenance | AB004879 |
| *Tcf7* | −2.74 | transcription factor 7, T-cell specific | transcription factor | cell growth/maintenance | AI019193 |
| *Map3k8* | −2.78 | mitogen activated protein kinase kinase kinase 8 | tyrosine kinase | cell growth/maintenance | D13759 |
| *Ssh3bp1* | −3.71 | spectrin SH3 domain binding protein 1 | signal transduction, actin binding | cell growth/maintenance | U17698 |
| *Tiam1* | −2.1 | T-cell lymphoma invasion and metastasis 1 | guanyl-nucleotide exchange factor | cell motility | AV331929 |
| *Krt1-13* | −2.9 | keratin complex 1, acidic, gene 13 | intermediate monomer | cytoskeleton/structural | X03492 |
| *Yy1* | −3 | YY1 transcription factor | transcription factor | developmental | M74590 |
| *Dntt* | −2.46 | deoxynucleotidyltransferase, terminal | DNA nucleotidyltransferase | DNA biosynthesis | AV312871 |
| *Prkdc* | −1.78 | protein kinase, DNA activated, catalytic polypeptide | DNA-dependent protein kinase | DNA damage repair | AB011543 |
| *Serpini1* | −2.86 | serine (or cysteine) proteinase inhibitor, clade I, member 1 | neural tissue | extracellular matrix remodeling | AJ001700 |
| *Pftk1* | −1.95 | PFTAIRE protein kinase 1 | S/T kinase | energy metabolism | AF033655 |
| *Ckm* | −2.22 | creatine kinase, muscle | creatine kinase | energy metabolism | AV086797 |
| *Ghrl-pending* | −2.78 | ghrelin | ligand | energy metabolism | AV206059 |
| *Slfn3* | −5.06 | schlafen 3 | lymphoid tissue | growth arrest | AF099974 |
| *Sel1h* | −1.79 | Sel1 (suppressor of lin-12) 1 homologue (*C. elegans*) | notch receptor activation growth | regulation | AF063095 |
| *Ash2l* | −2.35 | ash2 (absent, small, or homeotic)-like (*Drosophila*) | transcription factor | homeotic gene regulation | AV240479 |
| *Cd3z* | −2.19 | CD3 antigen, ζ polypeptide | receptor | immune response | J04967 |
| *Pglyrp* | −7.41 | peptidoglycan recognition protein | cytokine | immune response | AV092014 |
| *Pglyrp* | −10.72 | peptidoglycan recognition protein | cytokine | immune response | AF076482 |
| *Guca2* | −2.76 | guanylate cyclase activator 2 (guanylin 2, intestinal, heat stable) | ligand | ion-regulation | M95175 |
| *Ppap2a* | −1.87 | phosphatidic acid phosphatase 2a | acid phosphatase | lipid metabolism | D84376 |
| *Clcn7* | −2.11 | chloride channel 7 | voltage-gated ion channel | membrane transport | AI122121 |
| *Gabrr1* | −2.39 | γ-GABA-A receptor, subunit ρ1 | ligand-gated ion channel | membrane transport | AF024620 |
| *Aqp9* | −2.89 | aquaporin 9 | membrane channel | membrane transport | AA967194 |
| *Slc16a7* | −4.9 | solute carrier family 16 (monocarboxylic acid transporters), member 7 | carrier activity | membrane transport | AF058054 |
| *Gfi1* | −2.23 | growth factor independent 1 | transcription factor | morphogenesis | U58972 |
| *C1r* | −2.09 | complement component 1, r subcomponent | endopepdidase | protein processing | AV239653 |
| *Rab1* | −1.93 | RAB1, member RAS oncogene family | small GTPase | protein trafficking | AI853053 |
| *Hsp105* | −1.85 | heat shock protein | heat shock protein | stress response | L40406 |

NOTE: Microarray analysis of MMTV-ErbB2-$p27^{+/-}$ versus MMTV-ErbB2-$p27^{+/+}$ tumors. Genes up-regulated by affymetrix oligonucleotide array analysis. Direction and fold change are shown. Gene title and annotation description are listed. Data are shown with comparison to $p27^{Kip1}$ wild-type tumors. Thus, genes are up-regulated if there is increase in $p27^{+/-}$.

represented by rows and each experiment is shown as a column. Red and green denote increased and decreased expression levels, respectively, with the intensity reflecting the magnitude of change.

### PCR, RNA Extraction, Real-time PCR, Comparative Calculation, and Determination of Relative Expression Levels

**Validation of microarray gene expression results by real-time RT-PCR.** cDNA made from RNA extracted from animal tumor samples using standard guanidine isothiocyanate-phenol-chloroform method was subjected to GeneChip Mouse Expression Set 430 gene expression arrays (Affymetrix). The same RNA sample was RQ1 DNase I (Promega) treated and phenol-chloroform extracted before proceeding to validation of gene expression by real-time RT-PCR analysis. Equal quantities of DNA-free RNA were used for reverse transcription reactions for making cDNA using Iscript Reverse transcriptase kit (Bio-Rad, Hercules, CA). SYBR green–based real-time PCR reactions were done with QuantiTect SYBR Green PCR Kit and p27 primers (Prime Express 5.1, Applied Biosystems Inc., Foster City, CA; ref. 39) prevalidated QuantiTect Primer assays (Qiagen) for Cdc25a, Pglyrp1, Yy1, Col2a1, Cd97, Serpini1, Mmp16, Dusp9, Map3k8, Nfatc2, Mras, Tiam1, Epha2, and 18S RNA (internal control) on an 7900HT real-time PCR system (Applied Biosystems) using Sequence Detection System 2.1 with manufacturer-prescribed thermal cycling variables and real-time data collections points. All assays were set up for relative quantitation method where mean Ct values from $p27^{+/+}$ samples were used as calibrator for data analysis for $p27^{+/-}$ samples. The relative fold change of gene expression between $p27^{+/+}$ versus $p27^{+/-}$ was calculated using the standard $2^{-\Delta\Delta Ct}$ method.

### Fluorescence-Activated Cell Sorting Analysis

Small pieces of formalin preserved tumor samples were cut (~25-50 mg). Samples were rinsed (1-hour incubations) twice in water for a total of 2 hours at room temperature. Tissue was incubated overnight at 37°C with gentle agitation in a solution of pepsin and sodium chloride [0.5% pepsin, 0.9% NaCl (pH 1.5)]. Following incubation, the digested material was centrifuged at 5,000 × *g* for 5 minutes. The pellet was washed in PBS and repelleted, leaving 0.5 mL of PBS covering the cells. Citric acid buffer (96 parts sodium phosphate 0.2 mol/L and 4 parts citric acid 0.1 mol/L) was added to PBS in a 1:1 ratio and samples were incubated for 5 minutes. Cells were repelleted and the buffer was decanted. Cells were resuspended in a propidium iodide/RNase/PBS solution (final concentrations of 10 μg/mL propidium iodide and 60 μg/mL RNase). DNA content was then measured by flow cytometry using FACScan (Becton Dickinson Immunocytometry Systems, San Jose CA). Data were collected with ScanQuest software (Becton Dickinson) and analyzed with ModFit LT (Verity Software House, Inc., Topsham, ME).

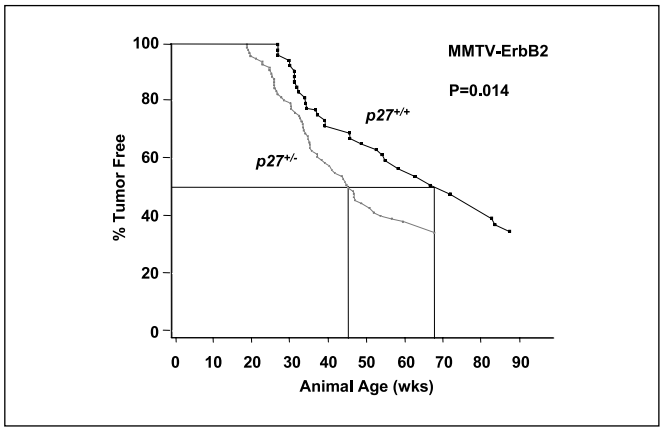


**Figure 1.** *In vivo* incidence of mammary tumor formation and survival in MMTV-ErbB2/$p27^{+/-}$ mice. *A,* mammary tumor onset rate in the MMTV-ErbB2/$p27^{+/+}$ and MMTV-ErbB2/$p27^{+/-}$ genotypes.

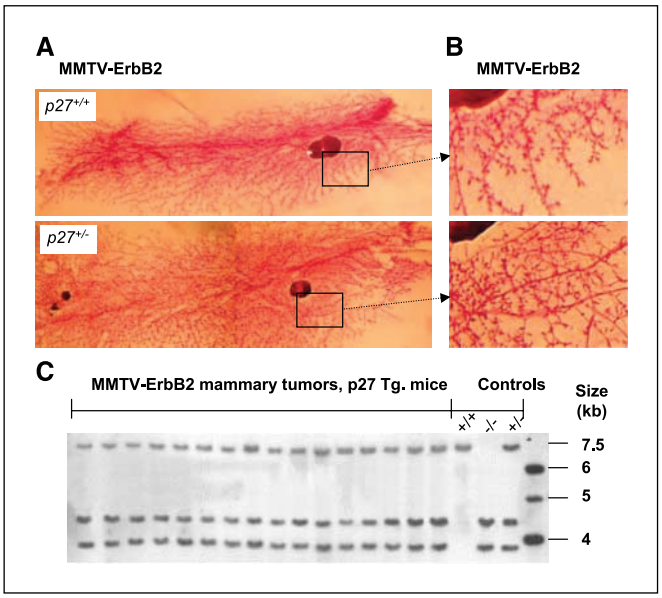


**Figure 2.** Mammary gland structure of ErbB2-$p27^{+/-}$ transgenic mice. Mammary gland whole mounts from MMTV-ErbB2/$p27^{+/+}$ and MMTV-ErbB2/$p27^{+/-}$ mice ($n$ = 10) were examined for ductal branching (mammary ducts/cm), mammary gland length (*A*) and mammary epithelial area (*B*), as described in Materials and Methods. *C,* genomic Southern blot analysis of mammary tumors derived from MMTV-ErbB2-$p27^{+/+}$ or MMTV-ErbB2-$p27^{+/-}$ mice (all tumors are heterozygous for the $p27^{Kip1}$ allele).

## Results

**Rapid onset of Neu-induced mammary tumors in $p27^{Kip1}$ heterozygote mice.** To examine the molecular mechanisms by which $p27^{Kip1}$ functions as a tumor suppressor with haploinsufficiency, transgenic mice were engineered. Experiments were conducted using transgenic mice lacking functional $p27^{Kip1}$ (17). Heterozygote *p27* mice were first bred into the FVB background to diminish any potential effects arising from the known, but poorly characterized, tumor-resistant phenotype of the C57BL/6 mice (40–42). Litters were then bred with MMTV-*neu* transgenic animals (FVB strain; ref. 24) to generate MMTV-*neu*-$p27^{+/+}$, MMTV-*neu*-$p27^{+/-}$, and MMTV-*neu*-$p27^{-/-}$ mice. Compared with the MMTV-*neu*-$p27^{+/+}$ mice, MMTV-*neu*-$p27^{+/-}$ mice were intermediate in size (data not shown), similar to previously published reports on $p27^{Kip1}$-deficient mice (17). The females from each genotype were monitored and palpated weekly for the onset of tumors. On detection, mammary tumors were periodically measured to determine growth rates before being carefully dissected free of surrounding tissues. MMTV-*neu*-$p27^{+/-}$ mice developed mammary gland tumors earlier and more rapidly than their littermates, with 50% having developed tumors ($T_{50}$) by 45 weeks of age (Fig. 1). In contrast, MMTV-*neu*-$p27^{+/+}$ mice exhibited a $T_{50}$ of 69 weeks. By the Cox proportional hazards model, MMTV-*neu*-$p27^{+/-}$ animals developed tumor onset significantly faster than the wild-type mice ($P$ = 0.014, compared with MMTV-*neu*-$p27^{+/+}$ mice). Previous studies have suggested a correlation between reduced $p27^{Kip1}$ levels and higher pathologic grade (8). Using the Annapolis classification system, histopathologic analysis was carried out to compare the *ErbB2*-$p27^{+/+}$ and *ErbB2*-$p27^{+/-}$ mammary tumors (43). The majority of the tumors were classified as undifferentiated adenocarcinomas with features of both glandular and squamous differentiation. The nuclei were slightly smaller than normal mammary epithelial nuclei but uniform in size

with delicate chromatin and abundant pink cytoplasm, characteristic of the ErbB2 histopathologic "signature" (43). As nuclear size is reported to correlate with specific genotypic and oncogenic changes (43), we formally measured nuclear size distribution within the ErbB2 mammary tumors from 30 separate animals. There was no significant alteration in nuclear size when tissues from the $p27^{+/-}$ and $p27^{+/+}$ tumors were compared ($n$ = 30 mice, $6 \times 10^4$ cells analyzed per sample; data not shown) and there was no difference in grade between the $p27^{+/-}$ and $p27^{+/+}$ mammary tumors (data not shown). DNA content analysis revealed that mammary tumors had remained diploid and that no significant differences in aneuploidy existed in the tumors due to the loss of a $p27^{Kip1}$ allele ($n$ = 40; data not shown).

The reduction in ErbB2-induced tumor onset of $p27^{+/-}$ versus $p27^{+/+}$ may have resulted from altered development of the mammary gland. The mammary gland architecture was therefore carefully analyzed by whole-mount mammary preparation, with measurements taken of ductal branching and length. Epithelial development was determined by cross-sectional area and total mammary gland size. Analysis was done at 166 days, at which time mammary gland maturation is complete. Comparison between the MMTV-ErbB2 $p27^{+/+}$ and MMTV-ErbB2 $p27^{+/-}$ animals revealed no significant difference in mammary gland length (3.66 $\pm$ 0.3 versus 3.78 $\pm$ 0.16 cm; $n$ = 10) and no significant decrease in the number of mammary duct branch points per centimeter of duct in the $p27^{+/-}$ mammary gland ($p27^{+/+}$ 33.9 $\pm$ 0.18 versus 30.70 $\pm$ 1.9 branches/cm duct; Fig. 2*A*). The mammary epithelium area of 10 separate animals was assessed with NIH image software and revealed no significant differences ($3.69 \times 10^4 \pm 0.37$ versus $3.72 \times 10^4 \pm 0.22$ arbitrary pixel units; Fig. 2*B*).

To determine whether the increase in tumor rate in $p27^{+/-}$ mice was secondary to either reduced expression of the *ErbB2* transgene or loss of the remaining $p27^{Kip1}$ allele, analysis was done on mammary tumors. Comparison was made between mammary tumor tissues derived from $p27^{+/+}$ and $p27^{+/-}$ transgenic mice (Fig. 2*C*). Genotyping for the $p27^{Kip1}$ allele and the MMTV-ErbB2 transgene was done with genomic Southern blotting and PCR analysis (data not shown). Analysis revealed that the $p27^{Kip1}$ allele status of the tumors had remained unchanged from that of the animal from which they were derived (Fig. 2*C*).

**Abundance of the SCF complex in MMTV-ErbB2 $p27^{+/-}$ mammary tumors.** Cyclin D1 is required for ErbB2-induced tumor growth in nude mice (25). We therefore examined the abundance and activity of the Cdks and Cdk inhibitors in the $p27^{+/+}$ and $p27^{+/-}$ ErbB2 mammary tumors. The abundance of these components was expressed as 100% in the $p27^{Kip1}$ wild-type for comparative purposes. Previous studies have shown an increased abundance of cyclin D1 in ErbB2 mammary tumors (25). Although cyclin D1 levels were increased compared with normal mammary epithelium, we found that the levels of cyclin D1 were similar between the $p27^{+/-}$ and $p27^{+/+}$ mammary tumors [protein abundance normalized to 100; 100 $\pm$ 5 ($p27^{+/+}$) versus 97 $\pm$ 6 ($p27^{+/-}$); $n$ = 20; Fig. 3*A*]. In the $p27^{+/-}$ mammary tumors, cyclin E levels were reduced by 60% [100 $\pm$ 23 ($p27^{+/+}$) versus 40 $\pm$ 14 ($p27^{+/-}$); $n$ = 20; Fig. 3*A*], $p27^{Kip1}$ levels were reduced by 80% [100 $\pm$ 25 ($p27^{+/+}$) versus 20 $\pm$ 5.9 ($p27^{+/-}$); $n$ = 18], and $p21^{Cip1}$ levels were reduced by 27% [100 $\pm$ 25 ($p27^{+/+}$) versus 73 $\pm$ 19 ($p27^{+/-}$); $n$ = 20; Fig. 3*B*].

$p27^{Kip1}$ is regulated at the level of translation and protein turnover, with $p27^{Kip1}$ ubiquitination by the SCF complex resulting in a 26S proteosome–mediated degradation. As $p27^{Kip1}$ levels were reduced by >50% in the ErbB2-$p27^{+/-}$ tumors when compared with the $p27^{+/+}$, we examined the abundance of the $SCF^{SKP2}$ components (Skp1, Cul1, and Skp2) as depletion of any specific factor prevents $p27^{Kip1}$ polyubiquitination and subsequent degradation (1–3, 44). The abundance of Skp1 and Cul1 were similar in the tumors from the $p27^{+/+}$ and $p27^{+/-}$ animals (data not shown). Skp2 levels were increased 5-fold in the $p27^{+/-}$ tumors (Fig. 3*C*). Tumors with increased Skp2 positively correlated with an earlier tumor onset time (Fig. 3*D*).

Skp2 levels were increased in the $p27^{+/-}$ tumors, correlating inversely with $p27^{Kip1}$ levels in murine ErbB2 tumors (Fig. 4*A*). To assess whether the relationship between Skp2 and $p27^{Kip1}$ advance in murine mammary tumors reflected changes in human breast cancer, studies were conducted. For analysis of human breast cancer tumors, immunohistochemical staining for Skp2 was done with a mix of four different affinity-purified mAbs as previously described (28). At least 20 high-power fields were chosen at random and 2,000 cells were counted. Skp2 levels were inversely concluded with $p27^{Kip1}$ abundance in human ErbB2-positive tumors (Fig. 4*B*). These findings suggest the increase correlation between Skp2 and $p27^{Kip1}$ levels in murine tumors may reflect changes in human ErbB2 breast cancer. We examined the relationship between Skp2 and $p27^{Kip1}$ levels and tumor onset with a three-dimensional pictograph. The three-dimensional modeling showed that high Skp2 and low $p27^{Kip1}$ levels correlated with earlier tumor onset in MMTV-ErbB2 tumors (Fig. 4*C*). Skp2 is induced during DNA synthesis. This prior observation raised

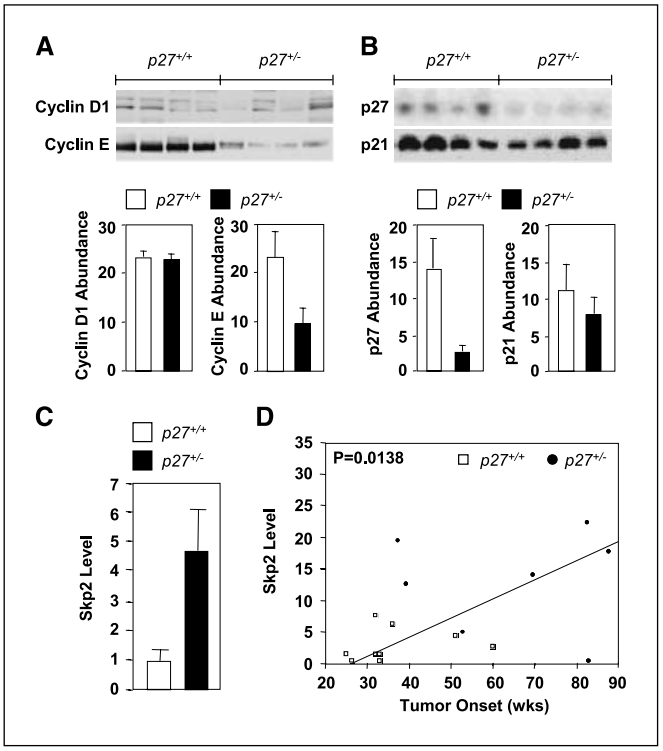


**Figure 3.** Loss of one $p27^{Kip1}$ allele increases Skp2 level in MMTV-ErbB2 mammary tumors. MMTV-ErbB2 mammary tumor lysates were analyzed by Western blotting for cyclin D1 and cyclin E ($n$ = 40; *A*) and $p27^{Kip1}$ and $p21^{Cip1}$ ($n$ = 40; *B*). *Columns,* mean protein abundance; *bars,* SE. *C,* Skp2 abundance determined by Western blotting of mammary tumors. *Columns,* mean ($n$ = 20); *bars,* SE. *D,* Skp2 abundance is increased in tumors with earlier onset.

the possibilities that the relationship between high Skp1 abundance and earlier tumor onset may simply reflect more rapidly proliferating tumors. The DNA synthetic phase fraction was therefore assessed in tumor samples with fluorescence-activated cell sorting analysis (45). The earlier-onset tumors did not have increased S-phase fractions (Fig. 4*D*); therefore, the increased Skp2 levels do not seem to result from increased DNA synthesis. Collectively, these analyses of murine and human tumors raised the possibility that $p27^{Kip1}$ may regulate Skp2 abundance.

To determine whether $p27^{Kip1}$ regulated Skp2 expression, the Skp2 promoter linked to a luciferase reporter gene was examined. Coexpression of an activating ErbB2 mutation enhanced Skp2 promoter activity by 50%. Coexpression of $p27^{Kip1}$ inhibited ErbB2 activation of Skp2 (Fig. 4*E*). Coexpression of Skp2 enhanced Skp2 promoter activity 5-fold (Fig. 4*F*). Coexpression of $p27^{Kip1}$ repressed Skp2 promoter activity 2-fold (Fig. 4*G*). Together these studies show that the Skp2 promoter is directly induced by ErbB2 and repressed by $p27^{Kip1}$.

To investigate further the role of $p27^{Kip1}$ in tumor onset in the mammary gland of the mouse, we determined the molecular genetic signature regulated by one allele of $p27^{Kip1}$ in mammary tumors using genome-wide expression analysis. Microarray analysis was conducted on ErbB2 $p27^{+/-}$ versus ErbB2 $p27^{+/+}$ mammary tumors. Tumors were taken from age-matched controls with similar tumor sizes. Both cDNA microarray and Affymetrix oligonucleotide microarray were used to expand the number of genes examined. We hypothesized that a subset of genes that were relevant to the earlier tumor formation would be different between these two genetically distinct sets of tumors and would include genes that are components of pathways involved in both growth promotion and growth inhibition. RNA was extracted from tumors that developed with the same $T_{50}$. Using the Affymetrix MG-U74AV2 mouse chip array (12,422 genes represented), microarray hybridization was done for each of six (three wild-type and three heterozygote) tumors. The mean expression levels of each gene were calculated for either the three wild-type or three heterozygote tumors. Mean differences that were statistically different ($P < 0.05$, Student's $t$ test) and showed a >1.8-fold change were scored. Using the $p27^{Kip1}$ heterozytote tumors as the reference, 72 identifiable genes were found to be differentially regulated (42 up-regulated

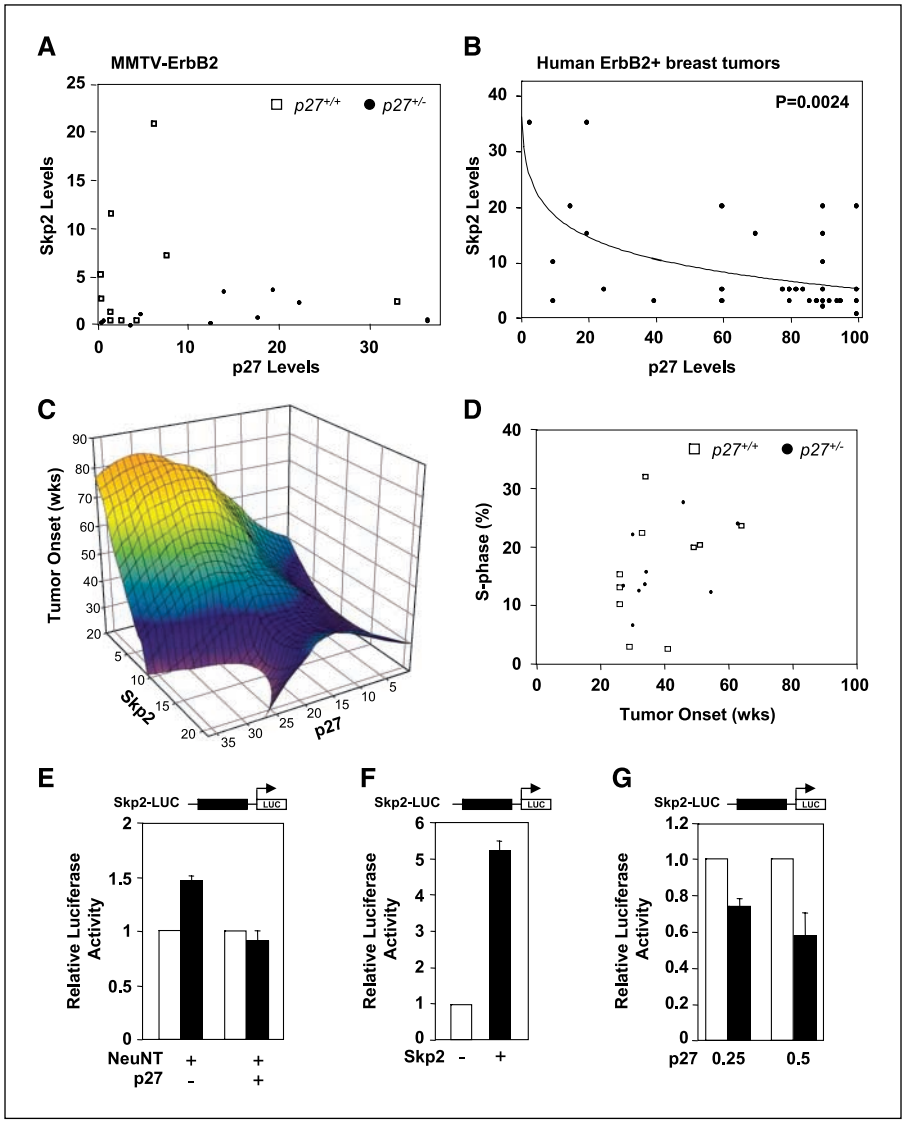


**Figure 4.** The SCF complex in the MMTV-ErbB2-$p27^{+/-}$ tumors. *A,* Skp2 and $p27^{Kip1}$ levels are inversely correlated in MMTV-ErbB2 mammary tumors and in human ErbB2 positive human breast cancers (Supplementary data; $n = 35$). *B,* Skp2 and $p27^{Kip1}$ levels are inversely correlated in the human ErbB2-positive human breast cancers ($n = 35$). *C,* three-dimensional pictograph of $p27^{Kip1}$, Skp2, and time of tumor onset, showing inverse correlation between Skp2 and $p27^{Kip1}$. *D,* the S phase of the ErbB2 tumors is shown with time of onset. *E,* the relative activity of the Skp2 promoter luciferase reporter was transfected into 3T3 cells in the presence of an activating mutant of ErbB2 (neu-NT) and $p27^{Kip1}$ or the expression vector for Skp2 (*G*) or $p27^{Kip1}$ (*F*) alone. *Columns,* mean ($n = 8$ separate transfections); *bars,* SE.

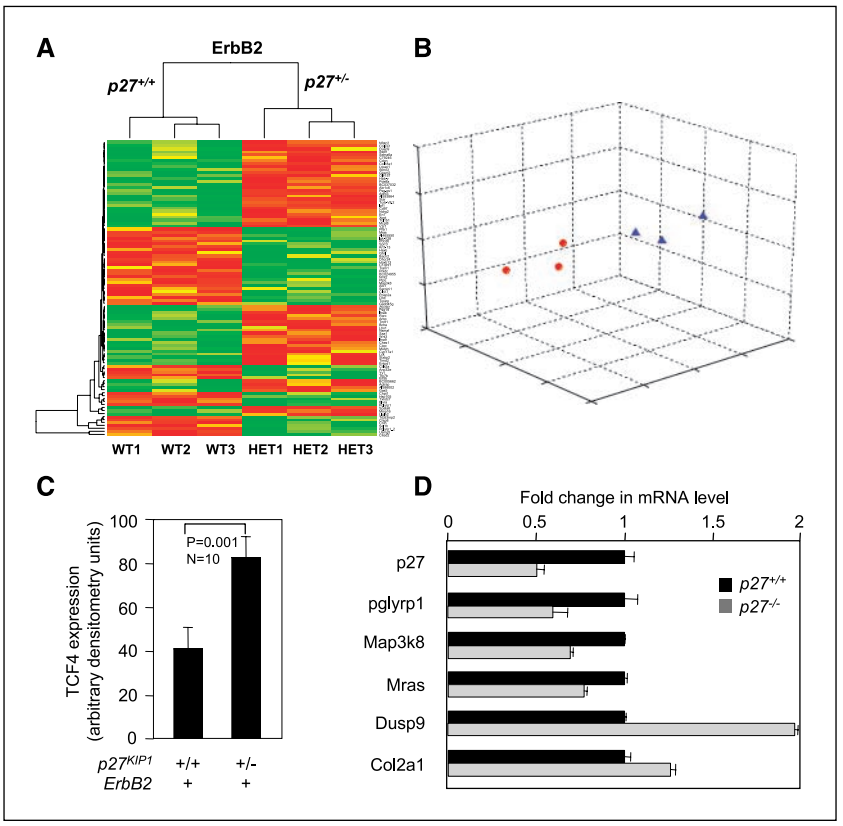


**Figure 5.** Microarray analysis of MMTV-ErbB2-$p27^{+/-}$ versus MMTV-ErbB2-$p27^{+/+}$ tumors. *A,* hierarchical cluster analysis for genes found to be differentially regulated. *Red,* up-regulation; *green,* down-regulation; *black,* no change. Each column represents a different tumor sample grouped together as those from $p27^{Kip1}$ wild-type animals (*left*) and those from $p27^{Kip1}$ heterozygote animals (*right*). Each row represents a different gene found to be differentially regulated. The tree branches define relationships between the various genes and between the tumors. The shorter the tree branch, the closer the similarity of the objects, as determined by hierarchical clustering (http://141.161.133.103/graph). *B,* multidimensional scaling analysis (*MDS*) for ErbB2/$p27^{Kip1}$ wild-type and heterozygote tumors. Distance between points on the three-dimensional scatter plot represents dissimilarities between tumors as determined from expression levels of 183 differentially expressed genes in each tumor sample. Graph plot positions are determined by applying the multidimensional scaling algorithm and are calculated from the Spearman's correlation measure ($r$) as $1 - r$. *C,* Western blot analysis of Tcf4. *Columns,* mean for $p27^{+/-}$ 10 wild-type and 10 ErbB2/$p27^{+/-}$ tumors; *bars,* SE. *D,* quantitative RT-PCR analysis of several genes altered in expression by microarray.

and 30 down-regulated; Fig. 5; Table 1). Within the up-regulated group of genes, nine were found to be involved in collaborative oncogenesis (Cdc25a, Wnt/β-catenin signaling; i.e., Wnt, Epha 2, matrix metalloproteases[11]; ref. 46) and cell growth/suvival, five in the immune response, four in membrane transport, three each in protein processing/trafficking and DNA or amino acid metabolism, and two genes were found to be associated with development.

Using a mouse cDNA chip array (8,969 genes represented), two microarray hybridizations were done for each of three wild-type versus $p27^{Kip1}$ heterozygote tumor comparisons (tumors from six different animals). For each hybridization, differences that were >1.8-fold were scored. Scored genes from each of the two hybridizations were then pooled. Genes considered to represent consistent differences were defined as differences that were present in two of the three comparisons. With the $p27^{Kip1}$ heterozygote tumors as a reference, 37 identifiable genes (Fig. 5*A*; Table 2) were found to be differentially regulated (34 up-regulated and 3 down-regulated). The cDNA array analysis extended the microarray analysis by detecting genes not represented or below the level of detection on the affymetrix MG-U74AV2 chip. Of the 34 up-regulated genes, 9 were categorized as functioning in cell growth, 4 were components of the immune response, and 2 were involved in cellular differentiation and protein or RNA processing. Comparison with previous studies indicated that the 19 genes that increased in the ErbB2 $p27^{+/-}$ tumors were previously identified to be increased in estrogen receptor–negative tumors (47, 48), and several genes induced in the ErbB2 $p27^{+/-}$ tumors were similar to previously described β-catenin-responsive genes (*EphA2, Claudin, aquaporin, matrix metalloproteinase, Tcf/Lef1,* $p27^{-/-}$ *β-catenin,* and *Engrailed2*; ref. 46).[11] To examine further the expression of genes altered by micoarray, we conducted Western blot analysis of Tcf4 as a marker for activation of β-catenin signaling. The *Tcf4* gene is induced by β-catenin and contributes to the induction of β-catenin signaling of downstream target genes (49). Western blot analysis was conducted on 20 tumors and the data are shown as mean densitometry indicating a >2-fold increase in Tcf4 and abundance in ErbB2/$p27^{+/-}$ tumor compared with ErbB2/$p27^{+/-}$ (Fig. 5*C*). Furthermore, analysis of several genes altered in expression by microarray was confirmed by RT-PCR analysis of mRNA from the mammary tumors (Fig. 5*D*). Collectively, the data of both array systems were consistent with a model in which p27 inhibited several collaborative oncogenic signaling pathways, including Cdc25a and Wnt/β-catenin signaling.

To examine the possibility that the induction of β-catenin-responsive genes in the ErbB2/$p27^{+/-}$ mammary tumors may be a function of reduced $p27^{Kip1}$ levels, we examined the possibility that $p27^{Kip1}$ may repress β-catenin signaling. Expression studies were conducted in $p27^{+/-}$ versus $p27^{+/-}$ cells. The transcription factor *Siamosis* is a β-catenin-responsive gene involved in the early dorsal ventral patterning (50). The *Siamosis* promoter was induced 5-fold by β-catenin S33 (Fig. 6*A*). Coexpression of $p27^{Kip1}$ repressed β-catenin-induced Siamosis luciferase reporter activity in wild-type and $p27^{-/-}$ cells (Fig. 6*B* and *C*). The Siamosis ΔTcf mutant, the c-myc Tcf mutant, and the Smad7 ΔTcf mutant were not repressed by $p27^{Kip1}$ (data not shown). The *c-myc* promoter was induced 4-fold by coexpression of β-catenin S33 as previously shown (51). The point mutant of the Tcf site was not induced by β-catenin S33 (Fig. 6*D*). Coexpression of $p27^{Kip1}$ inhibited β-catenin-induced

[11] http://www.stanford.edu/~rnusse/wntwindow.html.

**Table 2.** Differentially expressed genes: cDNA

| Symbol | Fold change | Gene assignment | Function/activity/tissue | Cluster category | GenBank accession no. |
|---|---|---|---|---|---|
| Genes up-regulated | | | | | |
| *Cldn6* | 1.83 | claudin 6 | tight junction adhesion function | cell adhesion | AA474499 |
| *Pdcd1* | 34.38 | programmed cell death 1 | receptor | cell death | X67914 |
| *Madh7/Smad7* | 4.93 | MAD homologue 7 (*Drosophila*) | TGF-β inhibitor | cell growth | AA022262 |
| *Fhl1* | 3.79 | four and a half LIM domains 1 | electron transporter activity | cell growth | AA047966 |
| *Pax5* | 2.68 | paired box gene 5 | transcription factor, B-cells | cell growth | M97013 |
| *Runx1* | 2.63 | runt related transcription factor 1 | transcription factor | cell growth | AA189661 |
| *Rrad* | 2.00 | Ras-related associated with diabetes | small monomeric GTPase | cell growth | AA450695 |
| *Pes1* | 2.00 | pescadillo homologue 1, containing BRCT domain (zebrafish) | ribosome biosynthesis | cell growth | AA003101 |
| *Mcpr* | 1.92 | meiotic check point regulator | meiosis | cell growth | AA003247 |
| *Bcl11a* | 1.89 | B-cell chronic lymphocytic leukemia/lymphoma 11A (zinc finger protein) | transcriptional co-repressor activity | cell growth | W99925 |
| *Lef1* | 4.96 | lymphoid enhancer binding factor 1 | transcription factor | cell growth/maintenance | X58636 |
| *Epb4.1* | 1.83 | erythrocyte protein band 4.1 | actin binding activity | cytoskeleton dynamics | AA014918 |
| *Rdh5* | 2.14 | retinol dehydrogenase 5 | retinol dehydrogenase | differentiation | AA275664 |
| *Dazl* | 2.00 | deleted in azoospermia-like | spermatozoa production | differentiation | AA414507 |
| *Ppt2* | 2.05 | palmitoyl-protein thioesterase 2 | thioesterase | fatty acid metabolism | AA008747 |
| *Blnk* | 2.61 | B-cell linker | antigen presentation | immune response | Y17159 |
| *B2m* | 2.20 | β-2 microglobulin | class 1 MHC component | immune response | AA109951 |
| *ligp-pending* | 2.17 | IFN-inducible GTPase | GTPase activity | immune response | AA277451 |
| *Btk* | 1.85 | Bruton agammaglobulinemia tyrosine kinase protein | tyrosine kinase | immune response | AA154035 |
| *Fxyd2* | 2.54 | FXYD domain-containing ion transport regulator 2 | modulates ATPase activity | membrane transport-ion | AA208297 |
| *Gal1-R* | 2.51 | expressed sequence tags, similar to MOUSE Galanin receptor type 1 (GAL1-R) | neuropeptide | neural communication | AA030752 |
| *Sepp1* | 1.89 | selenoprotein P, plasma, 1 | selenium transport in plasma | plasma ion transport | AA276440 |
| *ARM1/KLK4* | 2.57 | ADP-ribosylation factor-like membrane-associated protein Arm1 | serine protease | protein processing | AA015180 |
| *Cryac* | 2.40 | crystallin, αC | chaperone | protein processing | AA003272 |
| *2400002D02Rik* | 13.95 | RIKEN cDNA 2400002D02 gene | ribosomal recycling factor | protein synthesis | AA286398 |
| *B4galt5* | 6.85 | UDP-Gal:β-GlcNAc β1,4-galactosyltransferase, pp 5 | protein glycosylation | protein trafficking | AA021668 |
| *Car6* | 2.50 | carbonic anhydrase 6 | carbonic anhydrase | respiration | W11772 |
| *Cpsf2* | 2.54 | cleavage and polyadenylation specific factor 2 | RNA polyadenylation | RNA processing | AA002317 |
| *Dazap1* | 2.22 | DAZ associated protein 1 | RNA transport/localization | RNA processing | AA030214 |
| *Pscd1* | 2.12 | pleckstrin homologue Sec7 and coiled-coil domains 1 | guanyl-nucleotide release factor | signal transduction | AA422805 |
| *EIG180* | 2.43 | ethanol induced gene product EIG180 | | | AA002332 |
| *AI481750* | 2.17 | expressed sequence AI481750 | transcription factor | | W82945 |
| *Twistnb* | 2.00 | TWIST neighbor | | | AA172774 |
| *Hmg20b* | 1.94 | high mobility group 20 B | transcription factor/remodeling | | AA007769 |
| Genes down-regulated | | | | | |
| *Igfbp5* | −2.22 | insulin-like growth factor binding protein 5 | regulation of insulin-like growth factors | cell growth/maintenance | AA241784 |
| *Cpe* | −2.18 | carboxypeptidase E | carboxypeptidase | extracellular matrix dynamics | W83974 |
| *Bet1* | −2.26 | blocked early in transport 1 homologue (*S. cerevisiae*) | protein transport | protein trafficking | W18376 |

NOTE: Microarray analysis of MMTV-ErbB2-$p27^{+/-}$ versus MMTV-ErbB2-$p27^{+/+}$ tumors. Genes up-regulated by cDNA microarray analysis. Direction and fold change are shown. Gene title and annotation description are listed. Data is show with comparison to $p27^{Kip1}$ wild-type tumors. Thus, genes are up-regulated if increased in the $p27^{+/-}$.

*c-myc* promoter activity in both $p27^{-/-}$ and $p27^{+/+}$ 3T3 cells (Fig. 6*E* and *F*). Deletion of the Smad7 Tcf site increased luciferase activity 3-fold (Fig. 6*G*). The transfection of the activating β-catenin S33 enhanced activity of the Smad7 promoter 5-fold. Coexpression of $p27^{Kip1}$ repressed β-catenin-induced *Smad7* expression in a dose-dependent manner (Fig. 6*H*). In contrast, the Smad7 ΔTcf mutant was not activated by β-catenin. $p27^{Kip1}$ cotransfection repressed *Smad7* promoter activity in $p27^{Kip1}$ wild-type 3T3 cells (Fig. 6*I*). Together these studies show that $p27^{Kip1}$ inhibits β-catenin signaling to multiple distinct target genes.

## Discussion

Biallelic tumor-specific mutations have provided strong evidence of a causal link between tumorigenesis and several key tumor suppressors including *pRb, p53*, and *INK4a*. In the current studies, $p27^{Kip1}$ (*Cdkn1b*) functioned as a suppressor of ErbB2-induced mammary gland tumorigenesis. Analysis of the mammary tumors from the $p27^{+/-}$ mice showed that the remaining allele was expressed, suggesting that $p27^{Kip1}$ is haploinsufficient for tumor suppression. The ability of $p27^{Kip1}$ to function as a suppressor of ErbB2-induced mammary gland tumorigenesis with haploinsufficiency *in vivo* extends previous findings in which $p27^{Kip1}$ was haploinsufficient for suppression of chemical carcinogens or γ-irradiation-induced tumors and APC-mediated colonic carcinogenesis (52). The $p27^{+/-}$ mice in the FVB strain of the current studies developed mammary tumors with a $T_{50}$ not dissimilar to that of mice in the Bl6/FVB mixed strain in a prior study (53). Therefore, mice heterozygous for deletion of $p27^{Kip1}$, as has also been reported for transforming growth factor β(TGF-β; ref. 54) and *Dmp1* (55), show varying degrees of haploinsufficiency and do not conform to Knudson's two-hit model of tumor suppressors. Although only a handful of definitively haploinsufficient tumor suppressor genes have been identified, it has been recently argued that haploinsufficiency in some form may be a hallmark of essentially all tumor suppressors, although the mechanisms involved are unclear (56). The current studies showed that the loss of a single $p27^{Kip1}$ allele results in disproportionate loss of $p27^{Kip1}$ protein abundance and activates multiple distinct collaborative oncogenic signaling pathways. Global gene expression profiling and Western blot analysis of ErbB2/$p27^{+/-}$ tumors showed that the loss of $p27^{Kip1}$ induced genes promoting Wnt/β-catenin/hedgehog signaling (*Dhh, Wnt3*, and *Lef1*), lymphangiogenesis (*Flt3l* and *EphA2*), cellular proliferation, and collaborative oncogenic signaling (*Cdc25A, Smad7*, and *Skp2*). Reintroduction of $p27^{Kip1}$ into $p27^{Kip1}$-deficient cells inhibited expression of Skp2, Smad7, and Wnt/β-catenin responsive genes. Thus, $p27^{Kip1}$ inhibits Skp2, Smad7, and Wnt/β-catenin responsive genes through a mechanism that involves repression of target gene promoter activity.

Analysis of the molecular basis for the $p27^{Kip1}$ haploinsufficient mammary tumor suppression showed that the loss of one $p27^{Kip1}$ allele was associated with reduced $p27^{Kip1}$ levels correlating with earlier time of tumor onset. The accelerated loss of $p27^{Kip1}$ abundance on loss of a single allele may contribute to the acceleration of tumor onset in ErbB2/$p27^{+/-}$ mammary tumors. Reduced $p27^{Kip1}$ abundance correlates with poor prognosis in human breast cancer (6–9). $p27^{Kip1}$ degradation is mediated by the SCF complex following $p27^{Kip1}$ phosphorylation by cyclin E/Cdk2 (57). Herein, increased Skp2 abundance correlated with earlier onset of MMTV-ErbB2 tumors. Skp2 levels were substantially increased in the $p27^{+/-}$ tumors. Increased Skp2 correlated with

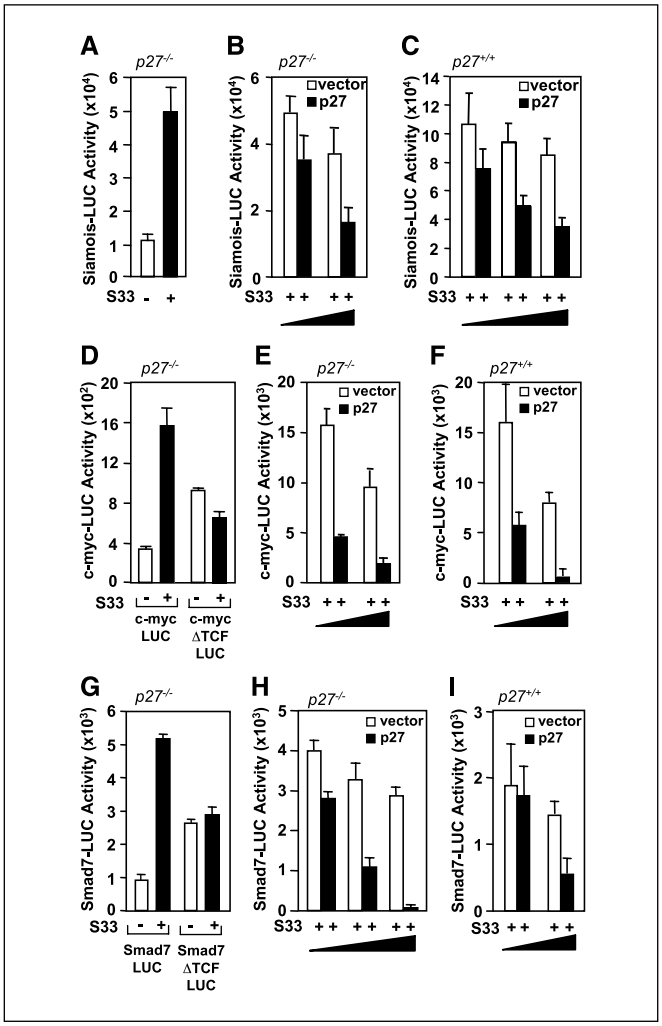


**Figure 6.** $p27^{Kip1}$ inhibits β-catenin signaling. *A*, the *Siamosis*-LUC reporter was assessed for β-catenin induction and $p27^{Kip1}$ regulation. *Columns,* mean relative light units × $10^3$ ($n$ = 9 separate experiments); *bars,* SE. *D* to *F*, the c-*Myc*-LUC reporter and c-*Myc* ΔTcf-LUC reporter were assessed for β-catenin responsiveness and regulation by cotransfected $p27^{Kip1}$. *G* to *I*, the *Smad7* promoter luciferase or Smad7 ΔTcf mutant was assessed for luciferase activity in the presence of activating β-catenin S33 and a transfected $p27^{Kip1}$ expression vector (*G*). Transfections were conducted in $p27^{+/+}$ (*I*) or $p27^{-/-}$ 3T3 (*H*) cells as indicated.

reduced $p27^{Kip1}$ levels in both murine and human breast tumors that overexpress ErbB2 (Fig. 4*A* and *B*), consistent with recent findings in human lymphomas, colorectal carcinoma, and oral squamous cell carcinomas (28, 58). Although Skp2 is induced during DNA synthesis, it is unlikely that the increase in Skp2 levels in the $p27^{+/-}$ tumors is a result of altered DNA synthesis per se, as S-phase fractions were similar between the $p27^{+/+}$ and $p27^{+/-}$ tumors. Herein Skp2 expression was repressed by $p27^{Kip1}$. Skp2 is a ubiquitylated target of Cul1, and Cul1 inhibits Skp2 expression (59). However, in the current studies, Cul1 levels were unchanged in mammary tumors of mice genetically heterozygous for $p27^{Kip1}$ (data not shown). As Skp2 abundance is normally induced by DNA synthesis and inhibited by Cul1, Skp2 abundance seems to be uncoupled from normal regulation in ErbB2 tumors. Skp2 promotes contact-independent growth (60); thus, such uncoupling with anomalous $p27^{Kip1}$ degradation would be predicted to contribute to the aberrant growth advantage. As cyclin E/Cdk2 kinase levels were 40% higher in the $p27^{+/-}$ tumors (not shown), it

would be anticipated that Skp2-mediated $p27^{Kip1}$ degradation would be more efficient in these tumors. Thus, it is unlikely that the increase in Skp2 is compensating for reduced ability to degrade its substrate. An alternative possibility is that Skp2 is induced by oncogenic stimuli and is contributing to the enhanced rate of tumorigenesis observed in the $p27^{+/-}$ tumors. In support of this hypothesis, increased Skp2 levels were found in murine mammary tumors with increased ErbB2 abundance, and oncogenic ErbB2 induced the Skp2 promoter. The current studies suggest that $p27^{Kip1}$ regulates its own abundance in the presence of ErbB2. The ability of $p27^{Kip1}$ to regulate Skp2 may contribute to the disproportionate loss of $p27^{Kip1}$ protein in the $p27^{Kip1}$ heterozygote mammary tumors.

Analysis of MMTV-ErbB2 $p27^{+/-}$ tumors showed that the genetic deletion of one $p27^{Kip1}$ allele induced multiple distinct collaborative oncogenic pathways (*Dhh, Wnt/β-catenin, Cdc25A, Skp2*, and *Smad7*). Cdc25A, Smad7, and Skp2 have each been shown to promote contact-independent growth (61–63). DUSP9, which encodes two $NH_2$-terminal CH2 domains homologous to Cdc25A (64), was, like Cdc25A, also induced in ErbB2/$p27^{+/-}$ tumors. $p27^{Kip1}$ deficiency increased expression of Dhh/Wnt/β-catenin responsive genes (Tcf, Ephrin receptor, Claudin, Wnt, aquaporin, and matrix metalloproteinases).[11] Semiquantitative RT-PCR analysis showed a 50% mean decrease in the mRNA abundance of $p27^{Kip1}$. Abundance of the β-catenin responsive gene *Tcf4* was increased >2-fold in ErbB2/$p27^{+/-}$ tumor, consistent with the model in which Tcf4 is itself induced by β-catenin signaling. Transcriptional activity of several β-catenin responsive promoters was increased in $p27^{-/-}$ cells in a Tcf site–dependent manner. Coexpression of $p27^{Kip1}$ repressed β-catenin-dependent activity. Ephrin receptors represent a large family of tyrosine kinases. The interactions between Eph receptors and their ligands involved direct cell-to-cell interactions, frequently resulting in repulsion and contributing to epithelial polarity (65). Ephrin receptor A2, which was induced in ErbB2/$p27^{+/-}$ mammary tumors, promotes tumor vascularization (66). Induction of β-catenin signaling promotes mammary tumorigenesis and induction of this pathway may have contributed to the more rapid onset of $p27^{Kip1}$-deficient ErbB2 mammary tumors.

Herein, tumors derived from mice genetically deleted of $p27^{Kip1}$ showed the induction of Dhh/Wnt/β-catenin signaling. β-Catenin is oncogenic in mouse models of tumorigenesis (67, 68) and β-catenin overrides density-dependent growth inhibition and cooperates with Ras in cellular transformation (69). How might $p27^{Kip1}$ inhibit expression of the Wnt/β-catenin pathway? The repression of β-catenin signaling by $p27^{Kip1}$ in mammary epithelial cells is consistent with findings that $p21^{Cip1}$ interrupts the β-catenin signaling pathway in intestinal cells (65). Activation of the Dhh/Wnt/β-catenin pathway is thought to expand the mammary gland stem cell compartment that contributes to tumorigenesis (70). In the current studies, $p27^{Kip1}$ repressed β-catenin signaling assayed in transient expression studies of multiple distinct Tcf target genes. We showed that the repression of β-catenin signaling by $p27^{Kip1}$ required the presence of the Tcf site in the promoter of the target genes assessed. The inhibition of β-catenin signaling by $p27^{Kip1}$ may likely contribute an antiproliferative component, the loss of which may in turn enhance the rate of onset of mammary tumorigenesis in the $p27^{Kip1}$ heterozygote mice.

## Acknowledgments

Received 1/16/2006; revised 5/31/2006; accepted 6/27/2006.

**Grant support:** NIH Cancer Center Core grant P30 CA56036-08; Canadian Breast Cancer Initiative and Medical Research Council of Canada Scientist award (W.J. Muller); NIH grants R01CA70896, R01CA75503, R01CA86072, and R01CA93596; Pfeiffer Foundation; Susan G. Komen Breast Cancer Foundation (R.G. Pestell); NIH grants AG20337C (C. Albanese) and CA536340 (J.C. Hulit); NIH training grants T32 DK 07513 (R.J. Lee), CA76642, and CA14462 (G. Inghirami); and Breast Cancer Alliance Inc. (A.A. Quong).

The costs of publication of this article were defrayed in part by the payment of page charges. This article must therefore be hereby marked *advertisement* in accordance with 18 U.S.C. Section 1734 solely to indicate this fact.

We thank Drs. E. Bottinger (Department of Medicine, Icahn Medical Institute, Mt. Sinai School of Medicine, New York, NY) and W. Tansey (Cold Spring Harbor Laboratories, Cold Spring Harbor, NY) for plasmids and Dr. M. Pagano for helpful discussions.

## References

1. Sutterluty H, Chatelain E, Marti A, et al. p45SKP2 promotes p27Kip1 degradation and induces S phase in quiescent cells. Nat Cell Biol 1999;1:207–14.
2. Rolfe M, Chiu MI, Pagano M. The ubiquitin-mediated proteolytic pathway as a therapeutic area. J Mol Med 1997;75:5–17.
3. Carrano A, Eytan E, Hershko A, Pagano M. SKP2 is required for ubiquitin-mediated degradation of the Cdk inhibitor p27. Nat Cell Biol 1999;1:193–9.
4. Zhang H, Kobayashi R, Galaktionov K, Beach D. p19Skp1 and p45Skp2 are essential elements of the cyclin A-CDK2 S phase kinase. Cell 1995;82:915–25.
5. Nakayama K, Nagahama H, Minamishima YA, et al. Targeted disruption of Skp2 results in accumulation of cyclin E and p27(Kip1), polyploidy and centrosome overduplication. EMBO J 2000;19:2069–81.
6. Catzavelos C, Bhattacharya N, Ung YC, et al. Decreased levels of the cell-cycle inhibitor p27Kip1 protein: Prognostic implications in primary breast cancer. Nat Med 1997;3:227–30.
7. Sgambato A, Zhang Y-J, Arber N, et al. Deregulated expression of p27Kip1 in human breast cancers. Clin Cancer Res 1997;3:1879–87.
8. Fredersdorf S, Burns J, Milne AM, et al. High level expression of p27kip1 and cyclin D1 in some human breast cancer cells: Inverse correlation between the expression of p27kip1 and degree of malignancy in human breast and colorectal cancers. Proc Natl Acad Sci U S A 1997;94:6380–5.
9. Porter PL, Malone KE, Heagerty PJ, et al. Expression of cell-cycle regulators p27Kip1 and cyclin E, alone and in combination, correlate with survival in young breast cancer patients. Nat Med 1997;3:222–5.
10. Ponce-Castañeda MV, Lee M-H, Latres E, et al. p27Kip1: chromosomal mapping to 12p12-12p13.1 and absence of mutations in human tumors. Cancer Res 1995;55:1211–4.
11. Kawamata N, Morosetti R, Miller CW, et al. Molecular analysis of the cyclin-dependent kinase inhibitor gene p27/Kip1 in human malignancies. Cancer Res 1995;55:2266–9.
12. Pietenpol JA, Bohlander SK, Sato Y, et al. Assignment of the human p27Kip1 gene to 12p13 and its analysis in leukemias. Cancer Res 1995;55:1206–10.
13. Stegmaier K, Pendse S, Barker GF, et al. Frequent loss of heterozygosity at the TEL gene locus in acute lymphoblastic leukemia of childhood. Blood 1995;86:38–44.
14. Hatta Y, Takeuchi S, Yokota J, Koeffler HP. Ovarian cancer has frequent loss of heterozygosity at chromosome 12p12.3-13.1 (region of TEL and Kip1 loci) and chromosome 12q23-ter: evidence for two new tumour-suppressor genes. Br J Cancer 1997;75:1256–62.
15. Slingerland J, Pagano M. Regulation of the cdk inhibitor p27 and its deregulation in cancer. J Cell Physiol 2000;183:10–7.
16. Weinstein IB. Disorders in cell circuitry during multistage carcinogenesis:the role of homeostasis. Carcinogenesis 2000;21:857–64.
17. Kiyokawa H, Kineman RD, Manova-Todorova KO, et al. Enhanced growth of mice lacking the cyclin-dependent kinase inhibitor function of p27Kip1. Cell 1996;85:721–32.
18. Fero ML, Rivkin M, Tasch M, et al. A syndrome of multiorgan hyperplasia with features of gigantism, tumorigenesis, and female sterility in p27Kip1-deficient mice. Cell 1996;85:733–44.
19. Nakayama K, Ishida N, Shirane M, et al. Mice lacking p27Kip1 display increased body size, multiple organ hyperplasia, retinal dysplasia, and pituitary tumors. Cell 1996;85:707–20.
20. Philipp-Staheli J, Kim KH, Payne SR, et al. Pathway-specific tumor suppression. Reduction of p27 accelerates gastrointestinal tumorigenesis in Apc mutant mice, but not in Smad3 mutant mice. Cancer Cell 2002;1:355–68.
21. Di Cristofano A, De Acetis M, Koff A, Cordon-Cardo C, Pandolfi PP. Pten and p27 KIP1 cooperate in prostate cancer tumor suppression in the mouse. Nat Genet 2001;27:222–4.
22. Slamon DJ, Clark GM, Wong SG, Levin WJ, Ullrich A, McGuire WL. Human breast cancer: correlation of relapse and survival with amplification of the HER-2/neu oncogene. Science 1987;235:177–82.
23. Muller WJ, Sinn E, Pattengale PK, Wallace R, Leder P. Single step induction of mammary adenocarcinoma in transgenic mice bearing the activated c-neu oncogene. Cell 1988;54:105–15.
24. Guy CT, Webster MA, Schaller M, Parson TJ, Cardiff RD, Muller WJ. Expression of the neu proto-oncogene in

the mammary epithelium of transgenic mice induces metastatic disease. Proc Natl Acad Sci U S A 1992;89:10578–82.
25. Lee RJ, Albanese C, Fu M, et al. Cyclin D1 is required for transformation by activated Neu and is induced through an E2F-dependent signaling pathway. Mol Cell Biol 2000;20:672–83.
26. Yu Q, Geng Y, Sicinski P. Specific protection against breast cancers by cyclin D1 ablation. Nature 2001;411:1017–21.
27. Yang HY, Zhou BP, Hung MC, Lee MH. Oncogenic signals of HER-2/neu in regulating the stability of the cyclin-dependent kinase inhibitor p27. J Biol Chem 2000;275:24735–9.
28. Latres E, Chiarle R, Schulman BA, et al. Role of the F-box protein Skp2 in lymphomagenesis. Proc Natl Acad Sci U S A 2001;98:2515–20.
29. Chiarle R, Budel LM, Skolnik J, et al. Increased proteasome degradation of cyclin-dependent kinase inhibitor p27 is associated with adecreased overall survival in mantle cell lymphoma. Blood 2000;95:619–26.
30. Albanese C, Wu K, D'Amico M, et al. IKKα regulates mitogenic signaling through transcriptional induction of cyclin D1 via Tcf. Mol Biol Cell 2003;14:585–99.
31. Brannon M, Gomperts M, Sumoy L, Moon RT, Kimelman D. A β-catenin/XTcf-3 complex binds to the siamois promoter to regulate dorsal axis specification in *Xenopus*. Genes Dev 1997;11:2359–70.
32. von Gersdorff G, Susztak K, Rezvani F, Bitzer M, Liang D, Bottinger EP. Smad3 and Smad4 mediate transcriptional activation of the human Smad7 promoter by transforming growth factor β. J Biol Chem 2000;275:11320–6.
33. Mendez J, Zou-Yang H, Kim S-Y, Hidaka M, Tansey WP, Stillman B. Human origin recognition complex large subunit is degraded by ubiquitin-mediated proteolysis after initiation of DNA replication. Mol Cell 2002;9:481–91.
34. Kim SY, Herbst A, Tworkowski KA, Salghetti SE, Tansey WP. Skp2 regulates Myc protein stability and activity. Mol Cell 2003;11:1177–88.
35. Shtutman M, Zhurinsky J, Simcha I, et al. The cyclin D1 gene is a target of the b-catenin/LEF-1 pathway. Proc Natl Acad Sci U S A 1999;96:5522–7.
36. Watanabe G, Howe A, Lee RJ, et al. Induction of cyclin D1 by simian virus 40 small tumor antigen. Proc Natl Acad Sci U S A 1996;93:12861–6.
37. Bearss DJ, Lee RJ, Troyer DA, Pestell RG, Windle JJ. Differential effects of p21(WAF1/CIP1) deficiency on MMTV-ras and MMTV-myc mammary tumor properties. Cancer Res 2002;62:2077–84.
38. Huang E, Ishida S, Pittman J, et al. Gene expression phenotypic models that predict the activity of oncogenic pathways. Nat Genet 2003;34:226–30.
39. Sakamaki T, Casimiro MC, Ju X, et al. Cyclin d1 determines mitochondrial function *in vivo*. Mol Cell Biol 2006;26:5449–69.
40. Drinkwater NR, Bennett LM. Genetic control of carcinogenesis in experimental animals. Prog Exp Tumor Res 1991;33:1–20.
41. Donehower LA, Godley LA, Aldaz CM, et al. Deficiency of p53 accelerates mammary tumorigenesis in Wnt-1 transgenic mice and promotes chromosomal instability. Genes Dev 1995;9:882–95.
42. DiGiovanni J. Genetic factors controlling responsiveness to skin tumor promotion in mice. Prog Clin Biol Res 1995;391:195–212.
43. Cardiff RD, Anver MR, Gusterson BA, et al. The mammary pathology of genetically engineered mice: the consensus report and recommendations from the Annapolis meeting. Oncogene 1999;19:968–88.
44. Tsvetkov LM, Yeh KH, Lee SJ, Sun H, Zhang H. p27(Kip1) ubiquitination and degradation is regulated by the SCF(Skp2) complex through phosphorylated Thr187 in p27. Curr Biol 1999;9:661–4.
45. Krishan A. Rapid flow cytofluorometric analysis of mammalian cell cycle by propidium iodide staining. J Cell Biol 1975;66:188–95.
46. van de Wetering M, Sancho E, Verweij C, et al. The β-catenin/TCF-4 complex imposes a crypt progenitor phenotype on colorectal cancer cells. Cell 2002;111:241–50.
47. van de Vijver MJ, He YD, van't Veer LJ, et al. A gene-expression signature as a predictor of survival in breast cancer. N Engl J Med 2002;347:1999–2009.
48. van't Veer LJ, Dai H, van de Vijver MJ, et al. Gene expression profiling predicts clinical outcome of breast cancer. Nature 2002;415:530–6.
49. Nateri A, Spencer-Dene B, Behrens A. Interaction of phosphorylated c-Jun with TCF4 regulates intestinal cancer development. Nature 2005;437:281–5.
50. Fan MJ, Gruning W, Walz G, Sokol SY. Wnt signaling and transcriptional control of Siamois in *Xenopus* embryos. Proc Natl Acad Sci U S A 1998;95:5626–31.
51. He TC, Sparks AB, Rago C, et al. Identification of c-MYC as a target of the APC pathway. Science 1998;281:1509–12.
52. Fero ML, Randel E, Gurley KE, Roberts JM, Kemp CJ. The murine p27Kip1 is haplo-insufficient for tumour suppression. Nature 1998;396:177–80.
53. Muraoka RS, Lenferink AEG, Simpson J, et al. Cyclin-dependent kinase inhibitor p27 Kip1 is required for mouse mammary gland morphogenesis and function. J Cell Biol 2001;153:917–31.
54. Tang B, Bottinger EP, Jakowlew SB, et al. Transforming growth factor-β1 is a new form of tumor suppressor with true haploid insufficiency. Nat Med 1998;4:802–7.
55. Inoue K, Zindy F, Randle DH, Rehg JE, Sherr CJ. Dmp1 is haplo-insufficient for tumor suppression and modifies the frequencies of Arf and p53 mutations in Myc-induced lymphomas. Genes Dev 2001;15:2934–9.
56. Quon KC, Berns A. Haplo-insufficiency? Let me count the ways. Genes Dev 2001;15:2917–21.
57. Montagnoli A, Fiore F, Eytan E, et al. Ubiquitination of p27 is regulated by Cdk-dependent phosphorylation and trimeric complex formation. Genes Dev 1999;13:1181–9.
58. Hershko D, Bornstein G, Ben-Izhak O, et al. Inverse relation between levels of p27(Kip1) and of its ubiquitin ligase subunit Skp2 in colorectal carcinomas. Cancer 2001;91:1745–51.
59. Wirbelauer C, Sutterluty H, Blondel M, et al. The F-box protein Skp2 is a ubiquitylation target of a Cul1-based core ubiquitin ligase complex: evidence for a role of Cul1 in the suppression of Skp2 expression in quiescent fibroblasts. EMBO J 2000;19:5362–75.
60. Pagano M, Tam SW, Theodoras AM, et al. Role of the ubiquitin-proteasome pathway in regulating abundance of the cyclin-dependent kinase inhibitor p27. Science 1995;269:682–5.
61. Carrano AC, Pagano M. Role of the F-box protein Skp2 in adhesion-dependent cell cycle progression. J Cell Biol 2001;153:1381–90.
62. Galaktionov K, Lee AK, Eckstein J, et al. CDC25 phosphatase as potential human oncogenes. Science 1995;269:1575–7.
63. Liu X, Lee J, Cooley M, Bhogte E, Hartley S, Glick A. Smad7 but not Smad6 cooperates with oncogenic ras to cause malignant conversion in a mouse model for squamous cell carcinoma. Cancer Res 2003;63:7760–8.
64. Christie GR, Williams DJ, Macisaac F, Dickinson RJ, Rosewell I, Keyse SM. The dual-specificity protein phosphatase DUSP9/MKP-4 is essential for placental function but is not required for normal embryonic development. Mol Cell Biol 2003;25:8323–33.
65. Batlle E, Henderson JT, Beghtel H, et al. β-Catenin and TCF mediate cell positioning in the intestinal epithelium by controlling the expression of EphB/EphrinB. Cell 2002;111:251–63.
66. Ogawa K, Pasqualini R, Lindberg RA, Kain R, Freeman AL, Pasquale EB. The ephrin-A1 ligand and its receptor, EphA2, are expressed during tumor neovascularization. Oncogene 2000;19:6033–42.
67. Gat U, DasGupta R, Degenstein L, Fuchs E. *De novo* hair follicle morphogenesis and hair tumors in mice expressing a truncated β-catenin in skin. Cell 1998;95:605–14.
68. Chan TA, Hermeking H, Lengauer C, Kinzler KW, Vogelstein B. 14-3-3 Sigma is required to prevent mitotic catastrophe after DNA damage. Nature 1999;401:616–20.
69. Damalas A, Kahan S, Shtutman M, Ben-Ze'ev A, Oren M. Deregulated β-catenin induces a p53- and ARF-dependent growth arrest and cooperates with Ras in transformation. EMBO J 2001;20:4912–22.
70. Li Y, Welm B, Podsypanina K, et al. Evidence that transgenes encoding components of the Wnt signaling pathway preferentially induce mammary cancers from progenitor cells. Proc Natl Acad Sci U S A 2003;100:15853–8.

# $p27^{Kip1}$ Repression of ErbB2-Induced Mammary Tumor Growth in Transgenic Mice Involves Skp2 and Wnt/ β-Catenin Signaling

James Hulit, Richard J. Lee, Zhiping Li, et al.

*Cancer Res* 2006;66:8529-8541.